# Supporting Information

# A Model Derived from Hydrodynamic Simulations for Extracting the Size of Spherical Particles from the Quartz Crystal Microbalance

Jurriaan J.J. Gillissen[1,2,4], Seyed R. Tabaei[1,2], Joshua A. Jackman[1,2], Nam-Joon Cho[*1,2,3]

[1]School of Materials Science and Engineering, Nanyang Technological University, 50 Nanyang Avenue 639798, Singapore
[2]Centre for Biomimetic Sensor Science, Nanyang Technological University, 50 Nanyang Drive 637553, Singapore
[3]School of Chemical and Biomedical Engineering, Nanyang Technological University, 62 Nanyang Drive 637459, Singapore

Present Address:
[4]Center for Environmental Sensing and Modeling (CENSAM) IRG Singapore-MIT Alliance for Research and Technology (SMART) Center, 3 Science Drive 2, Singapore 117543

*E-mail: njcho@ntu.edu.sg

## Supporting Section S1: Dimensional Analysis

We perform dimensional analysis to determine the general form of the relation between the various variables, which are at play in the hydrodynamic problem of a sphere attached to an oscillating wall, which are six in total, *i.e.*, the hydrodynamic force amplitude $\Delta\hat{F}_{\mathrm{H}}$, the velocity amplitude $\hat{U}$, the angular frequency $\omega$, the particle radius $a$, the fluid kinematic viscosity $\nu_{\mathrm{F}}$ and the fluid mass density $\rho_{\mathrm{F}}$. According to the Buckingham-Pi theorem,[1] one can combine six variables (with three units, being length, time and mass) into 6 – 3 = 3 independent dimensionless parameters $\hat{\Pi}_i = \Delta\hat{F}_H^{\alpha}\hat{U}^{\beta}\omega^{\gamma}a^{\delta}\nu_{\mathrm{F}}^{\varepsilon}\rho_F^{\zeta}$, where $i$ = 1, 2 or 3 and $\alpha$, $\beta$, $\gamma$, $\delta$, $\varepsilon$ and $\zeta$ are determined by demanding that $\hat{\Pi}_{\mathrm{i}}$ are dimensionless. This procedure results in the dimensionless force $\hat{\Pi}_1 = \Delta\hat{F}_{\mathrm{H}}/(\rho_F a^3\omega\hat{U})$, the dimensionless size $\Pi_2 = a\ \omega^{1/2}\nu_{\mathrm{F}}^{-1/2}$, and the dimensionless velocity $\hat{\Pi}_3 = \hat{U}a/\nu_F$, and the latter is also known as the Reynolds number Re, which is estimated to be Re = $10^{-2}$, based on $|\hat{U}|$ = $10^{-1}$ m s$^{-1}$, [2] $a$ = $10^{-7}$ m and $\nu_{\mathrm{F}}$ = $10^{-6}$ m$^2$s$^{-1}$. Since Re is small compared to unity, the hyrodynamics are independent of Re,

and the problem is therefore fully described by a single dimensionless, complex-valued function $\hat{\varphi}$ that relates the two remaining dimensionless variables $\widehat{\Pi}_1 = \hat{\varphi}(\Pi_2)$. By using the above definitions for $\widehat{\Pi}_1$ and $\Pi_2$ and $\delta = (2\nu_F/\omega)^{1/2}$, we write the governing relation as follows:

$$\Delta\hat{F}_H = i\rho_F a^3 \omega \hat{U} \hat{\varphi}\left(\frac{\delta}{a}\right), \tag{S1}$$

where $\delta$ is the viscous penetration depth and $\hat{\varphi}$ is a (yet unknown) dimensionless, complex valued function of a single dimensionless variable $\delta/a$. The imaginary unit has been added to Eq. (S1) to ensure that the real and imaginary parts of $\hat{\varphi}$ correspond to frequency shift and bandwidth shift, respectively.

## Supporting Section S2: Details of the Lattice Boltzmann Method

The Lattice Boltzmann (LB) method relies on solving the molecular probability density, which is a function of space, time and the molecular velocity, and evolves according to the Boltzmann equation.[3] Macroscopic quantities, such as the fluid velocity and the pressure, are moments of the velocity distribution function. The 3D space and time are discretized on a four dimensional hyper-cubic grid, with a spatial and temporal lattice spacing of $\Delta x$ and $\Delta t$, respectively. On each space-time lattice point, there is an additional discretization of the molecular velocity, which in this work involves 19 discrete velocities. Being a three-dimensional model (spatially) with 19 discrete velocities, this model is in the literature referred to as D3Q19.[3] The current LB scheme involves transporting probability densities between neighboring lattice nodes and relaxing them towards the Maxwell Boltzmann distribution, using the single relaxation time, collision model, which is in the literature referred to as the BGK collision model.[3]

As sketched in Fig. 1a in the main text, the fluid is bounded by six surfaces, on which boundary conditions are imposed. On the lower, bounding surface, which is the interface between the fluid and the solid substrate, we assume the no-slip boundary condition, which

means that the fluid velocity equals that of the substrate. On the upper, bounding surface we apply the free-slip condition, which means that the fluid can flow freely parallel to this surface, while it cannot penetrate this surface. In order to satisfy the free-slip condition on the top and the no-slip condition on the bottom (substrate; wall plus sphere), we employ the half-way, bounce-back method,[4] which approximates the shape of the sphere as a 3D staircase, which is illustrated in Fig. 1b in the main text.

On the remaining four bounding surfaces, which are normal to the horizontal directions, we impose periodic boundary conditions. Physically, this condition corresponds to a periodic arrangement of spheres on a horizontal square lattice with a spacing $L$. Since we are interested in the limit where the spheres do not couple hydrodynamically, we ensure, and validate in Section S4, that $L$ is sufficiently large compared to the sphere radius $a$ as well as to the viscous penetration depth $\delta$.

The LB method was implemented in FORTRAN and parallelized using the Message Passing Interface protocol.

**Supporting Section S3: Determining the QCM-D Force from the Simulation**

During simulation, we monitor the real valued hydrodynamic force $F_H$ ($t$) on the substrate using two methods. The first method involves surface integrating the momentum exchange between the fluid and the substrate, by evaluating changes in the LB probability during bounce-back.[5] The second method is based on the integral fluid momentum balance, which is obtained by taking the volume integral of Eq. (3) in the main text:

$$F_H = \rho_F V_F \omega \left|\widehat{U}\right| \sin(\omega t) - \frac{dP_F}{dt}, \qquad \text{(S2)}$$

where $V_F$ and $P_F$ are the total volume and the total momentum of the fluid in the computational domain, respectively. We compute the difference $\Delta F_H(t)$ between the hydrodynamic force on the substrate $F_H$ (sphere plus wall) minus the hydrodynamic force on

the wall without the sphere $L^2\left|\widehat{U}\right|\rho_F\sqrt{2\omega\nu_F}\cos\left(\omega t+\frac{\pi}{4}\right)$. [6] Fig. S1 shows $\Delta F_{\mathrm{H}}(t)$ as a function of time for four simulations corresponding to $\delta/a$ = 0.6, 1.2, 2.3 and 4.6, respectively. The total force $\Delta F$ acting on the QCM-D (particle inertia force plus hydrodynamic force) is computed by adding the inertia of the sphere $-\omega\left|\widehat{U}\right|\sin(\omega t)m_p$ to $\Delta F_{\mathrm{H}}(t)$. Here $L$ is the horizontal domain size (inter-particle spacing), $\left|\widehat{U}\right|$ is the absolute value of the quartz surface velocity amplitude, $\rho_{\mathrm{F}}$ is the fluid mass density, $\omega = 2\pi f$ is the quartz angular frequency, $m_{\mathrm{P}} = (4\pi/3)\rho_{\mathrm{P}}a^3$ is the particle mass and $\rho_{\mathrm{P}}$ is the particle mass density, respectively. The corresponding (complex-valued) QCM-D force amplitude $\Delta\hat{F}$ [defined in Eq. (1) in the main text] is computed by Fourier transformation of $\Delta F(t)$ between $T < t < 2T$, where $T = 1/f$ is the oscillation period. The real and imaginary parts of $\Delta\hat{F}/i\widehat{U}$ correspond to the QCM-D frequency and bandwidth shifts; see Eq. (1) in the main text.

**Supporting Section S4: Accuracy of the Numerical Simulation**

The accuracy of the simulation depends on the grid resolution $a/\Delta x$ and on the relative domain size $L/a$ or $L/\delta$. The grid resolution must be sufficient, such that the surface of the sphere is accurately represented by the staircase approximation (see Fig. 1b in the main text), and the domain size $L$ must be large enough compared to the sphere radius $a$, and compared to the viscous penetration depth $\delta$, such that there is negligible hydrodynamic coupling between the sphere and its periodic images and negligible effect of the unphysical free-slip condition at the upper surface.

In this work, we use $a/\Delta x$ = 10 - 20 and $L/a$ = 8 – 32 (see Table S1) and we verify here that these values guarantee sufficient numerical accuracy. Since there is no analytical or reference solution available for the hydrodynamics of a sphere on an oscillating wall, we first study the accuracy of the method by considering two alternative flow configurations, for

which analytical solutions are available. These configurations are that of the steady shear flow past a sphere attached to a wall and that of an oscillating sphere in a stagnant fluid in the absence of walls. These problems contain essentially the same physics and numerical challenges as the actual problem of a sphere attached to an oscillating wall.

The steady shear test problem is simulated by placing a sphere on the bottom wall of the cubical, computational domain and placing a second, no-slip wall at the top of the domain, which is moving with a velocity $\gamma L$ in the $x$ direction. Here $\gamma$ is the shear rate and $L$ is the domain height. Periodic conditions are applied on the remaining four boundaries. At the start of the simulation, the fluid velocity profile is assumed to be linear, *i.e.*, $u_x\,(t = 0) = \gamma z$, which corresponds to the profile between two moving walls in the absence of the sphere. During the flow simulation, we measure the hydrodynamic force $\Delta F_H$ on the sphere as a function of time, which is shown in Fig. S2a. As can be seen in that figure and also in Table S2, the scaled force $\Delta F_H/(6\pi a^2 \eta_F \gamma)$ converges to an asymptotic value, which is within 3% of the theoretical value of 1.7.[6]

Next, we discuss the test case of an oscillating sphere in a stagnant fluid in the absence of walls. Here, we place a sphere in the center of the computational domain, which is periodic on all six boundaries. Similar to the case of the flow around the sphere on the oscillating wall, we solve this problem in a reference frame that oscillates with the sphere by adding an oscillating body force to the equation of motion [see Eq. (3) in the main text]. At the start of the simulation, the fluid is at rest. During the simulation, we measure the force on the sphere by using two methods. The first method involves summing the hydrodynamic stress over the surface elements of the sphere,[4] and the second is based on the acceleration of the fluid as a whole [see Eq. (S2)]. Fig. S2b shows that both methods produce a nearly identical time-dependent force, which validates the implementation of the co-moving reference frame. We measure the complex-valued amplitude of the hydrodynamic force oscillation by Fourier

transformation of the force signal over one period $T = 1/f$, between $T < t < 2T$. Table S3 shows, that, for the present numerical parameters, the real and imaginary parts of the simulated, complex force amplitude are within 10 % and 2 % of the analytical solution, respectively. [7]

In addition to these analytical test cases, we consider the grid-convergence of the simulation of the sphere on the oscillating wall, by comparing the simulation outcome to a second series of simulations, in which we doubled the grid resolution in each direction. As reported in Table S1, we find that for $\delta/a < 4$, the numerical solutions on both grids are within 1% of each other for the frequency shift and within 10% of each other for the bandwidth shift. The bandwidth shift is more prone to numerical inaccuracy than the frequency shift because the bandwidth shift is a few-fold smaller than the frequency shift. These results support that for $\delta/a < 4$, the domain is sufficiently large and the grid is sufficiently fine, such that the numerical solution is, to a reasonable extent, independent of these numerical parameters.

**Supporting Section S5: Diffusion Limited Adsorption Model**

Here we derive a model for the number $N$ of adsorbed vesicles onto the QCM-D surface: $\mathrm{d}N/\mathrm{d}t = A_Q J$, where $A_Q = \pi W^2/4 = 97$ mm$^2$ is the QCM-D substrate area, $W = (4/\pi)(A_Q)^{1/2} = 11$ mm is the diameter of the cylindrical QCM-D measurement chamber and $J = cD/h$ is the particle flux onto the surface, which is assumed to be limited by diffusion.[8,9] The particle number density in the bulk $c = c_m N_A a_L^2/(8 M_L a^2) = 6 \times 10^{17}$ m$^{-3}$ is estimated by dividing the number of lipid molecules per unit volume of solution by the number of lipid molecules in the bilayer of a single vesicle, where it is assumed that each lipid occupies an area in the membrane $\pi a_L^2$, that is equal to that in a planar bilayer. The particle diffusivity $D = k_B T/(6\pi\eta_F a)$ is modeled using the Stokes-Einstein relation, and the particle-concentration-

boundary-layer-thickness $h = (DWH/V)^{1/3}$ is modeled using flat plate boundary layer theory.[10] Here $N_A$ is Avogadro's number, $a_L$ = 0.45 nm is the cross-sectional radius of one lipid molecule, [11] $M_L$ = 786 g/mol is the molecular weight of DOPC lipid, $k_BT$ is the Boltzmann energy, $V = Q/WH$ is the fluid velocity, $Q$ = 50 μL/min is the volumetric flow rate through the QCM-D chamber, and $H$ =0.6 mm is the height of the cylindrical QCM-D measurement chamber, respectively. Combining the above equations shows that $N$ increases linearly in time:

$$N \approx 0.13cQ^{1/3}\left(\frac{k_BTA_Q}{a\eta_F H}\right)^{2/3} t. \qquad \text{(S3)}$$

Eq. (S3) is based on two main approximations: (i) estimating the number of lipid molecules per vesicle, by considering the area per lipid in a flat bilayer configuration and (ii) approximating the diffusion-limited adsorption flux, using flat plate boundary layer theory, while ignoring the geometrical details of the QCM-D flow chamber. The latter assumption probably introduces the most uncertainty, and the model can at best be considered an order of magnitude estimate.

## Supporting Section S6: Experimental Materials & Methods

### Vesicle Preparation

Small unilamellar vesicles (SUVs) were prepared from 5 mg/mL 1,2-dioleoyl-*sn*-glycero-3-phosphocholine (DOPC) lipid in an aqueous buffer solution with 10 mM Tris [pH 7.5] and 150 mM NaCl by extrusion through a polycarbonate membrane with either 30, nm 50 nm, 100 nm or 200 nm pores (Mini Extruder, Avanti Polar Lipids, Alabaster, AL). The vesicles are referred to as SUV1, SUV2, SUV3 and SUV4, and their properties are summarized in Table 1 in the main text. The nominal (intensity weighted) radius $a$ of the vesicles is measured by dynamic light scattering (90Plus Particle Size Analyzer, Brookhaven Instrument Corporation, Holtsville, NY), resulting in $a$ = 27 nm, 38 nm, 57 nm and 78 nm, respectively.

The corresponding size distributions are provided in Fig. S4. All solutions were prepared using Milli-Q-treated water with a minimum resistivity of 18.2 MΩ·cm (Millipore, Billerica, MA, USA). Immediately before the QCM-D experiment, the vesicles were diluted to $c_m$ = 0.05 mg/mL for SUV2 and $c_m$ = 0.005 mg/mL for SUV1, SUV3 and SUV4 and in a 10 mM Tris buffer, with a NaCl concentration of either 75 or 250 mM.

QCM-D Experiments

A Q-Sense E4 QCM-D instrument (Biolin Scientific AB, Stockholm, Sweden) was used to monitor SUV adsorption onto an AT-cut, piezoelectric, quartz crystal, with a fundamental frequency of $f_0$ = 5 MHz and a sputter-coated, 50-nm thick layer of titanium (model no. QSX 310, Biolin Scientific AB). A peristaltic pump (Reglo Digital, Ismatec, Glattbrugg, Switzerland) was used to inject liquid samples into the cylindrical measurement chamber (diameter $W$ = 11 mm, area $A_Q$ = 97 mm$^2$, and height $H$ = 0.6 mm) at a flow rate of $Q$ = 50 µL/min. The temperature in the measurement chamber was maintained at 25.0 ± 0.5 °C. The experimental data were collected at the 3$^{rd}$ to 11$^{th}$ odd overtones using the QSoft software program (Biolin Scientific AB).

**Table S1. Numerical parameters and results of the simulations of a sphere attached to an oscillating wall.** $a$ is the particle radius, $\Delta x$ is the grid spacing, $L$ is the horizontal domain size, $L_z$ is the vertical domain size, $\delta = (\nu_F/\pi f)^{1/2}$ is the viscous penetration depth, $\nu_F = \Delta x^2/(6\Delta t)$ is the fluid kinematic viscosity, $\rho_F$ is the fluid mass density, $f$ is the oscillation frequency, $\omega = 2\pi f$ is the oscillation angular frequency, $\hat{U}$ is the complex-valued velocity amplitude and $\Delta\hat{F}$ is the complex-valued QCM-D force amplitude [defined in Eq. (1) in the main text], where the real part $\Re(\Delta\hat{F}/i\hat{U})$ corresponds to the frequency shift and the imaginary part $\Im(\Delta\hat{F}/i\hat{U})$ corresponds to the bandwidth shift. Simulations are carried out for $\delta/a$ between 0.6 and 4.6. The computed relation between $\Delta\hat{F}$ and $\delta/a$ is given in Fig. 3 in the main text. The numerical accuracy of the simulations for $\delta/a < 3$ is verified by comparing results on a relatively coarse grid (open circles in Fig. S3) to results on a relatively fine grid (plusses in Fig. S3), where the number of grid points has been doubled in each direction.

| Marker Fig. S3 | $\delta/a$ | $L_z/\delta$ | $a/\Delta x$ | $L/\Delta x$ | $L_z/\Delta x$ | $f\,\Delta t$ | $\Re\left(\frac{\Delta\hat{F}}{i\rho_F a^3\omega\hat{U}}\right)$ | $\Im\left(\frac{\Delta\hat{F}}{i\rho_F a^3\omega\hat{U}}\right)$ |
|---|---|---|---|---|---|---|---|---|
| o | 0.576 | 22.2 | 20 | 160 | 256 | $4\times10^{-4}$ | 12.55 | 3.22 |
| + | 0.576 | 22.2 | 40 | 320 | 512 | $1\times10^{-4}$ | 12.52 | 3.87 |
| o | 1.15 | 11.1 | 10 | 80 | 128 | $4\times10^{-4}$ | 17.16 | 5.33 |
| + | 1.15 | 11.1 | 20 | 160 | 256 | $1\times10^{-4}$ | 17.15 | 5.89 |
| o | 2.30 | 5.56 | 10 | 160 | 128 | $1\times10^{-4}$ | 24.40 | 6.98 |
| + | 2.30 | 5.56 | 20 | 320 | 256 | $0.25\times10^{-4}$ | 24.63 | 7.67 |
| n.a. | 4.61 | 5.56 | 10 | 320 | 256 | $0.25\times10^{-4}$ | 33.67 | 6.90 |

**Table S2. Validation of the numerical method for the steady shear flow past a sphere attached to a wall.** $a$ is the particle radius, $\Delta x$ is the grid spacing, $L$ is the domain size (same in all three directions), $\Delta F_H$ is the simulated hydrodynamic force on the sphere, $\gamma$ is the shear rate and $\eta_F$ is the fluid dynamic viscosity. The %Error corresponds to the difference between the simulated value and the analytical solution.[6]

| $a/\Delta x$ | $L/a$ | $\Delta F_H/6\pi\eta_F a^2\gamma$ Simulation | $\Delta F_H/6\pi\eta_F a^2\gamma$ %Error |
|---|---|---|---|
| 5 | 13 | 1.740 | 2.4% |
| 10 | 26 | 1.685 | 0.87% |

**Table S3. Validation of the numerical method for an oscillating sphere in the absence of walls.** $a$ is the particle radius, $\Delta x$ is the grid spacing, $L$ is the domain size (same in all three directions) and $\hat{F}_H$ is the complex-valued, simulated, hydrodynamic force amplitude, where the real part $\Re(\hat{F}_H/\mathrm{i}\hat{U})$ is in phase with the displacement oscillation and the imaginary part $\Im(\hat{F}_H/\mathrm{i}\hat{U})$ is opposite to the velocity oscillation, $\hat{U}$ is the velocity amplitude and $\eta_F$ is the fluid dynamic viscosity. For this test case, we used $a/\delta = 0.22$, where $\delta = (\nu_F/\pi f)^{1/2}$ is the viscous penetration depth, $\nu_F = \eta_F/\rho_F$ is the fluid kinematic viscosity, $\rho_F$ is the fluid mass density and $f$ is the oscillation frequency. The %Error corresponds to the difference between the simulated value and the analytical solution. [7]

| $a/\Delta x$ | $L/a$ | $\Re\left(\frac{\hat{F}_H}{i6\pi\eta_F a\hat{U}}\right)$ Simulation | $\Re\left(\frac{\hat{F}_H}{i6\pi\eta_F a\hat{U}}\right)$ Analytical | $\Re\left(\frac{\hat{F}_H}{i6\pi\eta_F a\hat{U}}\right)$ %Error | $\Im\left(\frac{\hat{F}_H}{i6\pi\eta_F a\hat{U}}\right)$ Simulation | $\Im\left(\frac{\hat{F}_H}{i6\pi\eta_F a\hat{U}}\right)$ Analytical | $\Im\left(\frac{\hat{F}_H}{i6\pi\eta_F a\hat{U}}\right)$ %Error |
|---|---|---|---|---|---|---|---|
| 5 | 13 | 0.241 | 0.265 | 9.3% | 1.215 | 1.217 | 1.7% |
| 10 | 26 | 0.493 | 0.531 | 7.2% | 1.419 | 1.434 | 1.1% |

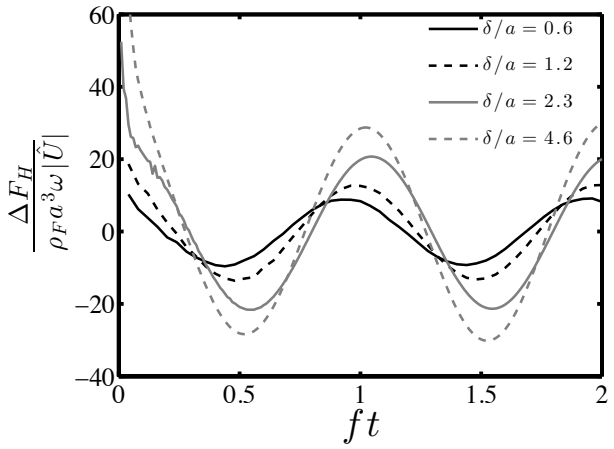


**Supporting Fig. S1. Numerical simulation of a sphere attached to an oscillating wall.** The hydrodynamic force $\Delta F_H/(\rho_F a^3 \omega |\widehat{U}|)$ due to the adsorption of a sphere on the QCM-D surface, as a function of scaled time $ft$ for various scaled viscous penetration depths $\delta/a$. $\rho_F$ is the fluid mass density, $a$ is the sphere radius, $|\widehat{U}|$ is the absolute value of the quartz velocity amplitude, $\delta = (\nu_F/\pi f)^{1/2}$ is the viscous penetration depth, $\nu_F$ is the fluid kinematic viscosity, $f$ is the oscillation frequency and $\omega = 2\pi f$ is the oscillation angular frequency.

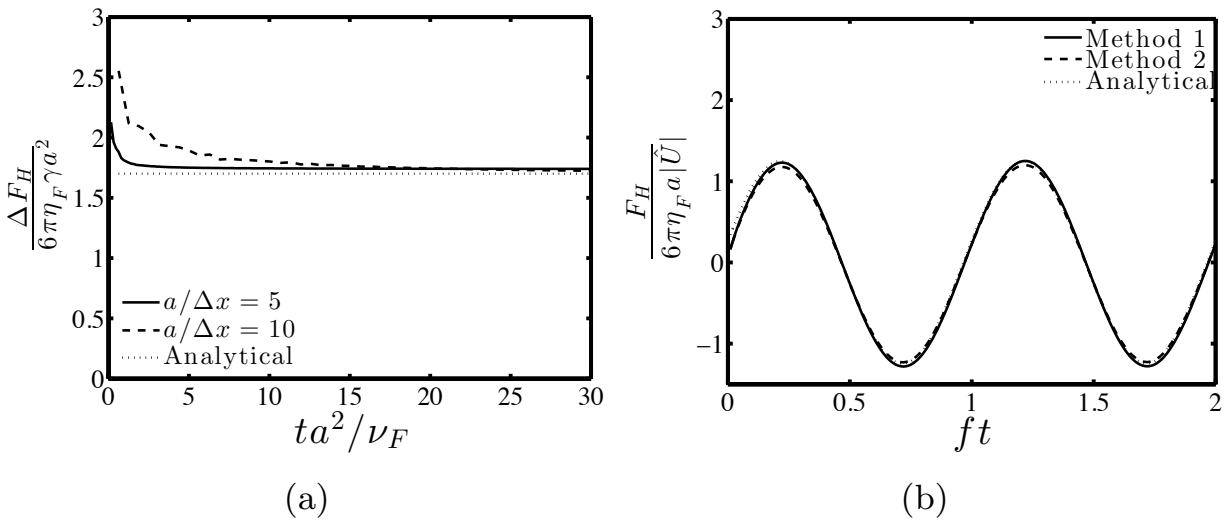


**Supporting Fig. S2. Validation of the numerical method.** (a) Steady shear flow past a sphere attached to a wall**.** The scaled hydrodynamic force $\Delta F_H/(6\pi\eta_F a^2\gamma)$ on the sphere, as a function of the scaled time $ta^2/\nu_F$. $\eta_F$ is the fluid dynamic viscosity, $a$ is the sphere radius, $\gamma$ is the shear rate and $\nu_F$ is the fluid kinematic viscosity. Further numerical parameters are given in Table S2. The solid and the dashed lines correspond to a grid resolution of $a/\Delta x$ = 5 and 10, respectively, where $\Delta x$ is the lattice spacing. The dotted line corresponds to the analytical solution.[6] (b) Oscillating sphere in the absence of walls. The scaled hydrodynamic force $F_H/(6\pi\eta_F a|\widehat{U}|)$ on the sphere, as a function of the (scaled) time $ft$ for a grid resolution (number of grid points per sphere radius) of $a/\Delta x$ = 5 and a scaled particle size of $a/\delta$ = 0.22. Here $\delta = (\nu_F/\pi f)^{1/2}$ is the viscous penetration depth and $f$ is the oscillation frequency. Further numerical parameters are given in Table S3. The hydrodynamic force is computed by summing the hydrodynamic stress over the surface elements of the sphere [solid line; Method 1][4] or by summing the acceleration of the fluid over the domain [dashed line; Method 2; Eq. (S2)]. The dotted line corresponds to the analytical solution. [7]

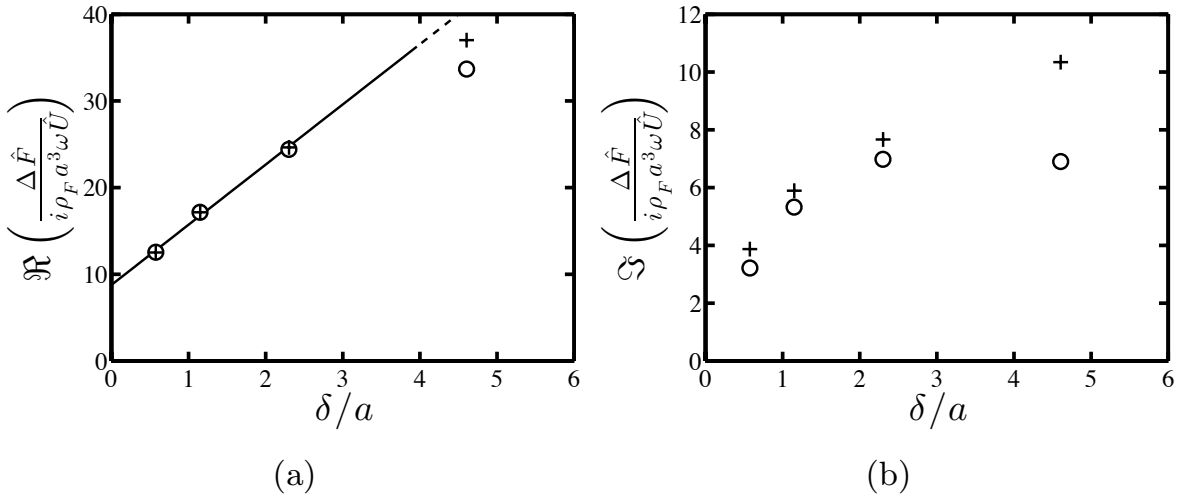


**Supporting Fig. S3. Validation of the numerical method.** Real (inertia) part (a) and imaginary (friction) part (b) of the scaled QCM-D force due to the adsorption of a sphere as a function of the scaled viscous penetration depth $\delta/a$. Here, $\Delta\hat{F}$ is the complex-valued QCM-D force amplitude [defined in Eq. (1) in the main text], $\rho_F$ is the fluid mass density, $\omega$ is the angular frequency, $\hat{U}$ is the complex-valued velocity amplitude of the quartz, $a$ is the particle radius and $\delta$ is the viscous penetration depth. Comparison between results on relatively coarse grid (open circles) and a relatively fine grid (plusses). Parameters are given in Table S1.

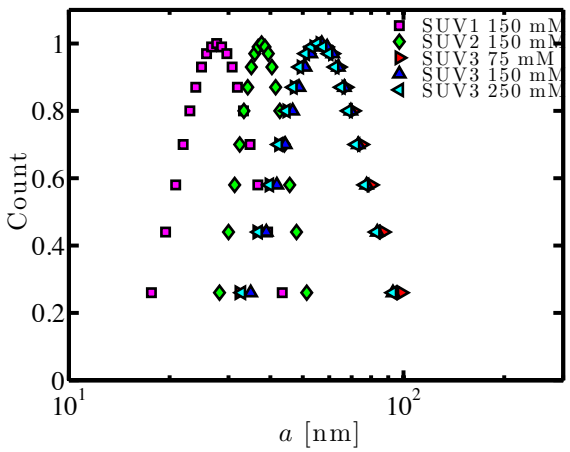


**Supporting Fig. S4. Vesicle size distribution obtained from dynamic light scattering (DLS).** Vesicles are produced by mixing lipids with an aqueous buffer solution with 150 mM ionic strength and extruding the mixture through a membrane with a nominal pore size of 30, 50 or 100 nm, referred to SUV1, SUV2 and SUV3, respectively. DLS data of SUV2 show no significant difference when dissolved in different ionic strengths.

**Supporting Movie S1.** Fluid velocity vector field in *xz*-plane intersecting a sphere that is attached to an oscillating wall. The sphere radius $a$ equals eight lattice spacings and the scaled penetration depth equals $\delta/a = 1.3$. For clarity, only part of the computational domain is shown. The animation shows that, with each cycle, a vortex is formed and released from the top of the sphere.

**Supporting References**


1. G. I. Barenblatt, *Scaling, self-similarity, and intermediate asymptotics: dimensional analysis and intermediate asymptotics*, Cambridge University Press, 1996.
2. A. Arnau, *Piezoelectric transducers and applications*, Springer, 2008.
3. S. Succi, *The lattice Boltzmann equation: for fluid dynamics and beyond*, Oxford university press, 2001.
4. A. Ladd and R. Verberg, *Journal of Statistical Physics*, 2001, **104**, 1191-1251.
5. R. Mei, D. Yu, W. Shyy and L.-S. Luo, *Physical Review E*, 2002, **65**, 041203.
6. M. O'Neill, *Chemical Engineering Science*, 1968, **23**, 1293-1298.
7. L. D. Landau and E. M. Lifshitz, *Fluid Mechanics*, Pergamon Press, Oxford, UK, 1959.
8. V. Zhdanov, C. Keller, K. Glasmästar and B. Kasemo, *The Journal of Chemical Physics*, 2000, **112**, 900-909.
9. C. Keller, K. Glasmästar, V. Zhdanov and B. Kasemo, *Physical Review Letters*, 2000, **84**, 5443-5446.
10. H. Schlichting, *Boundary-layer theory*, McGraw-Hill, 1968.
11. R. Merkel, E. Sackmann and E. Evans, *Journal de Physique*, 1989, **50**, 1535-1555.